

MoS<sub>2</sub> as an ideal material for valleytronics:  
valley-selective circular dichroism and valley Hall effect

December 20, 2011

Ting Cao,<sup>1</sup> Ji Feng,<sup>1†</sup> Junren Shi,<sup>1</sup> Qian Niu<sup>2</sup> & Enge Wang<sup>1\*</sup>

<sup>1</sup>International Center for Quantum Materials, Peking University, Beijing, China 100871. <sup>2</sup>Department of Physics, University of Texas, Austin, TX

178712, USA. <sup>†</sup>E-mail: jfeng11@pku.edu.cn. \*E-mail:

egwang@pku.edu.cn

## ABSTRACT

A two-dimensional honeycomb lattice harbors a pair of inequivalent valleys in the  $\mathbf{k}$ -space electronic structure, in the vicinities of the vertices of a hexagonal Brillouin zone,  $\mathbf{K}_{\pm}$ . It is particularly appealing to exploit this emergent degree of freedom of charge carriers, in what is termed “valleytronics”,<sup>1-3</sup> if charge carrier imbalance between the valleys can be achieved. The physics of valley polarization will make possible electronic devices such as valley filter and valley valve, and optoelectronic Hall devices,<sup>4;5</sup> all very promising for next-generation electronic and optoelectronic applications. The key challenge lies with achieving valley imbalance, of which a convincing demonstration in a two-dimensional honeycomb structure remains evasive, while there are only a handful of examples for other materials.<sup>6-9</sup> We show here, using first principles calculations, that monolayer MoS<sub>2</sub>, a novel two-dimensional semiconductor with a 1.8 eV direct band gap,<sup>10;11</sup> is an ideal material for valleytronics by valley-selective circular dichroism<sup>5</sup>, with ensuing valley polarization and valley Hall effect.

A non-equilibrium charge carrier imbalance between valleys is the key to creating valleytronic devices. The principal mechanism invoked here is circularly polarized optical excitation.<sup>4;5</sup> In this approach, the two valleys absorb left- and right-handed photons differently, a phenomenon referred to as circular dichroism (CD). In order to obtain the valley-selective CD, it is essential then to break the inversion symmetry of the honeycomb lattice. In the case of graphene, it was suggested that by interacting graphene with a substrate such that the center of inversion can be obliterated, whereupon a gap opens up in each valley.<sup>12;13</sup> This strategy, however, is quite challenging experimentally. And even in the eventual realization, there can only be a weak perturbation to graphene via the weak covalent coupling at large van der Waals separations.<sup>13</sup>

Since its first isolation, monolayer MoS<sub>2</sub> has attracted immense attention. Many measurements have been performed to characterize the optical and transport properties of this material.<sup>10;11;14-16</sup> In monolayer MoS<sub>2</sub>, two layers of sulfur atoms in a two-dimensional hexagonal lattice are stacked over each other in an eclipsed fashion. Each Mo sits in the center of a trigonal prismatic cage formed by 6 sulfur atoms ([Fig.1a](#)). Quite remarkably in the context of current discussion, the natural stable structure of free-standing monolayer MoS<sub>2</sub> is a honeycomb lattice with inequivalent bipartite coloring, breaking the inversion symmetry (see [Fig.1b](#)). Bulk MoS<sub>2</sub> has an indirect band gap. Interestingly, when thinned to the monolayer limit the material acquires direct band gaps located exactly at the corners of the Brillouin zone. Indeed, with its 1.8 eV direct band gap and unique two-dimensional structure embracing the high-symmetry valleys, monolayer MoS<sub>2</sub> has much to offer in the exploration of novel electronic and optoelectronic devices and the associated physics. It is

quite natural to question whether it is possible to achieve valley-selective CD in this semiconducting atomic membrane, which will endow electrons in this material the valley degree of freedom, in addition to charge and spin that have been routinely explored in conventional device physics.

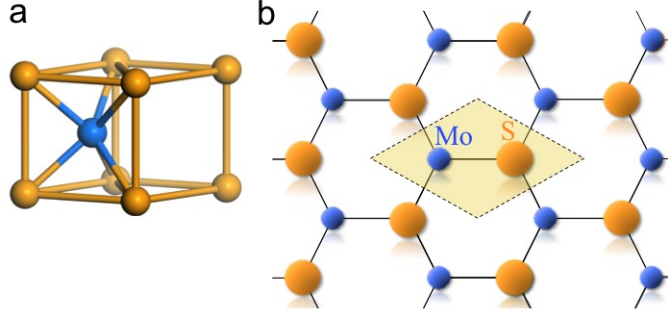


Figure 1: The crystal structure of monolayer MoS<sub>2</sub>. (a) Coordination environment of Mo in the structure. (b) A top view of the lattice, emphasizing the connection to a honeycomb lattice. In our calculations, we use an optimized structure at the level of local density approximation in density functional theory (see text). The shaded region bounded by dashed lines corresponds to one primitive cell. The unit cell parameter is  $a = 3.12 \text{ \AA}$ , and the vertical separation between sulfur layers is  $3.11 \text{ \AA}$ .

The key quantity to assess is, therefore, the  $\mathbf{k}$ -resolved degree of optical polarization,  $\eta(\mathbf{k})$ , between the top of the valence bands and the bottom of the conduction bands<sup>5</sup>

$$\eta(\mathbf{k}, \omega_{cv}) = \frac{|\mathcal{P}_+^{cv}(\mathbf{k})|^2 - |\mathcal{P}_-^{cv}(\mathbf{k})|^2}{|\mathcal{P}_+^{cv}(\mathbf{k})|^2 + |\mathcal{P}_-^{cv}(\mathbf{k})|^2}. \quad (1)$$

This quantity is the difference between the absorption of left- and right-handed lights ( $\pm$ ), normalized by total absorption, at each  $\mathbf{k}$ -point and evaluated between the top of the valence bands ( $v$ ) and the bottom of conduction bands ( $c$ ).

Note that the dependence on the transition energy,  $\hbar\omega_{cv}(\mathbf{k}) = \epsilon_c(\mathbf{k}) - \epsilon_v(\mathbf{k})$ , is implicit through  $\mathbf{k}$ . Here, the transition matrix element of circular polarization is  $\mathcal{P}_{\pm}^{cv}(\mathbf{k}) = \frac{1}{\sqrt{2}}[P_x^{cv}(\mathbf{k}) \pm iP_y^{cv}(\mathbf{k})]$ . The interband matrix elements,  $\mathbf{P}^{cv}(\mathbf{k}) = \langle \psi_{c\mathbf{k}} | \hat{\mathbf{p}} | \psi_{v\mathbf{k}} \rangle$ , are evaluated using the density functional perturbation theory (DFPT), within the local density approximation (LDA),<sup>17</sup> as implemented in VASP.<sup>18</sup> Spin-orbit coupling is not included in our calculations. Briefly, a planewave basis set is employed at a cut-off energy 600 eV, and a total of 80 bands are included to ensure convergence of all computed quantities. A very dense  $\mathbf{k}$ -point mesh ( $123 \times 123$  grid points) over the reducible two-dimensional full Brillouin zone is sampled in our calculations.

As shown in Fig.2a chiral absorption selectivity is indeed exact at  $\mathbf{K}_{\pm}$  with  $\eta = \pm 1$ . The contrast in the chiral absorptivities between the valleys owes its origin in the symmetry of both lattice and local atomic orbitals, which is quite different from the gapped graphene case<sup>5</sup>. A band state relevant to the optical excitation originates from local atomic states (or more generally, Wannier functions) bearing different orbital magnetic quantum numbers,  $l$ . In this case, the states at the top of the valence bands involve only  $d_{x^2-y^2}$  and  $d_{xy}$  on Mo, and  $p_x$  and  $p_y$  states on S. At  $\mathbf{K}_+$ , the  $d$ -states on Mo hybridize as  $\frac{1}{\sqrt{2}}(d_{x^2-y^2} + id_{xy})$  ( $l = +2$ ) to interact with  $\frac{1}{\sqrt{2}}(p_x + ip_y)$  ( $l = +1$ ). At  $\mathbf{K}_-$ , the  $d$ -states on Mo hybridize as  $\frac{1}{\sqrt{2}}(d_{x^2-y^2} - id_{xy})$  ( $l = -2$ ) to interact with  $\frac{1}{\sqrt{2}}(p_x - ip_y)$  ( $l = -1$ ). At the bottom of the conduction band, only  $d_{z^2}$  state on Mo ( $l = 0$ ) is involved. These atomic orbitals form such linear combinations in accordance with the  $D_{3h}$  point group symmetry and the lattice translational symmetry.

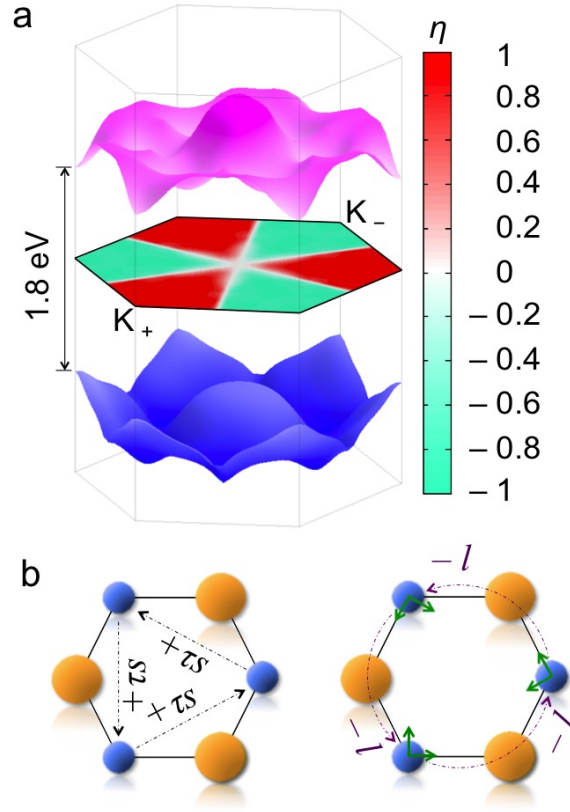


Figure 2: Valley-selective circular dichroism of monolayer MoS<sub>2</sub>. (a) Top valence band (blue) and bottom conduction band (pink). The center hexagon is the Brillouin zone color-coded by the degree of circular polarization,  $\eta(\mathbf{k})$ , as defined in the text. The vector connecting  $\mathbf{K}_+$  and  $\mathbf{K}_-$  is perpendicular to Mo-S bond in the crystal structure in (a). (b) Schematic of phase winding on the MoS<sub>2</sub> lattice that gives rise to the chiral optical selectivity. Left panel: the contribution to phase winding from the Bloch lattice phase, where  $\tau = \pm 1$  is the valley index, and  $s = 1, 2$  corresponding to the Mo and S sites (isospin). Right panel: the phase winding under a three-fold rotation. The green axes indicate the rotation of local atomic coordinates that leads to the azimuth dissynchronization.

The optical selection rule is rooted in the phase winding of the Bloch states under rotational symmetry, 3-fold rotation ( $\hat{C}_3$ ) in this case. Given the symmetry-adapted linear combination orbitals, the azimuthal phase associated with the 3-fold rotation at  $\mathbf{K}_\pm$  is readily calculable,

$$\hat{C}_3|v(\mathbf{K}_\pm)\rangle = |v(\mathbf{K}_\pm)\rangle, \quad (2)$$

$$\hat{C}_3|c(\mathbf{K}_\pm)\rangle = e^{\mp i2\pi/3}|c(\mathbf{K}_\pm)\rangle \quad (3)$$

where  $v$  and  $c$  correspond to the valence and conduction band extrema, respectively. Notice, however, the phase winding associated with the rotation has two distinct contributions. The first comes from the Bloch phase shift in stepping from one lattice site to the next, as in the case of gapped graphene.<sup>4</sup> The second phase factor arises as a consequence of dissynchronization of the azimuthal phase (associated with the magnetic quantum number,  $l$ ) concomitant with rotation of the local atomic coordinates. These are schematically illustrated in [Fig.2b](#).

Now the chiral optical selectivity of the valleys can be deduced. The bottom of the conduction bands at the valleys, dominated by the  $l = 0$   $d$ -states on Mo, bears an overall azimuthal quantum number  $m_\pm = \pm 1$ , at  $\mathbf{K}_\pm$ . At the top of the valence bands,  $m_\pm = 0$ . Then for an optical transition at  $\mathbf{K}_\pm$ , the angular momentum selection rule indicates that  $\Delta m_\pm = \pm 1$ , corresponding to the absorption of left- and right-handed photons. Therefore, our DFPT results concerning the close neighborhood of the valleys, which are the most important to the proposed optical valley polarization, are in fact ensured by the symmetry of the material.

There is an important distinction, compared to gapped graphene, in the microscopic origin of chiral optical selection rule; that is, the selectivity arises

directly from the local relative azimuthal phase of the atomic orbitals, in contrast to the sublattice-dependent Bloch phase winding in the case of gapped graphene.<sup>4</sup> The bonding in the electronic states in MoS<sub>2</sub> across the gap is also considerably more complex, exhibiting richer possibilities of variation owing to the symmetry of local atomic states. Remarkably, the selectivity is nearly perfect over the entire valleys, and only changes sign rapidly across valley boundaries (Fig.2a). This is to say, the entire valley  $\mathbf{K}_+$  absorbs almost purely left-handed photons, whereas the entire valley  $\mathbf{K}_-$  purely right-handed. The perfect valley-contrasting CD is very much conducive to optical polarization of the valleys.

Now that we have established the valley-selective CD in monolayer MoS<sub>2</sub>, it is also interesting to look at the Berry curvature,  $\Omega_n(\mathbf{k})$ , which, if present, has crucial influence on the transport properties. Of note, Berry curvature enters into the semiclassical wavepacket dynamics via an anomalous velocity perpendicular to the applied electric field ( $\sim \mathbf{E} \times \Omega_n(\mathbf{k})$ ), in addition to the usual group velocity of Bloch bands.<sup>19;20</sup> The presence of non-vanishing Berry curvature is possible in the non-centrosymmetric honeycomb lattice.<sup>4</sup> In Fig.3, we plot the Berry curvature,  $\Omega_{n\mathbf{k},z} = -2\text{Im}\langle \partial u_{n\mathbf{k}}/\partial k_x | \partial u_{n\mathbf{k}}/\partial k_y \rangle$  along the  $\mathbf{K}_- - \Gamma - \mathbf{K}_+$  path. Since the system has time-reversal symmetry and not inversion symmetry,  $\Omega_n(\mathbf{k})$  is an odd function in  $\mathbf{k}$  with generally non-zero values, as expected. The charge carriers' anomalous velocity acquires opposite signs in the two valleys, exactly canceling each other's contribution to the transverse current. At equilibrium, freestanding monolayer MoS<sub>2</sub> will not exhibit anomalous Hall effect. Notice that at  $\mathbf{K}_\pm$ , the Berry curvatures do not have the particle-hole symmetry. This is a clear indication that the physics of MoS<sub>2</sub> cannot be fully captured by a minimalistic two-band model, as distinct



from the case of gapped graphene.<sup>4;21</sup>

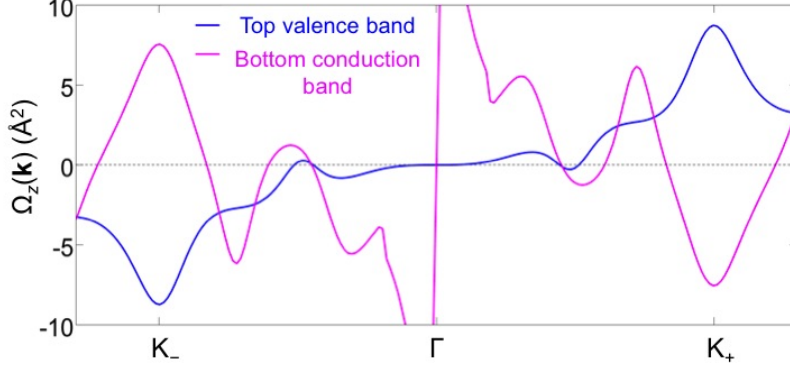


Figure 3: Berry curvature,  $\Omega_z(\mathbf{k})$ , of bands across the band gap. The Berry curvature of only the states along the  $\mathbf{K}_- - \Gamma - \mathbf{K}_+$  path of the Brillouin zone are plotted. Notice that the value of Berry curvature is large for the conduction band at the zone center, where bands are degenerate.

When valley polarization is induced by, say, valley-selective CD, only one valley has non-vanishing charge carrier population. This can then lead to the valley Hall effect.<sup>5</sup> The Berry curvature across the band edges near  $\mathbf{K}_\pm$  is most relevant to photo excited charge carriers. We see that at the band edges both conduction and valence bands display significant Berry curvature with opposite signs. Consequently, when electrons and holes are generated by a circularly polarized irradiation, both types of charge carriers have an intrinsic *concurrent* contribution to the Hall conductivity. Our results indicate that valley Hall effect in this material indeed warrants experimental assaying. In closing, we also would like to point out that MoS<sub>2</sub> is but one of the many transition metal dichalcogenides, MX<sub>2</sub>, where M = Mo, W, and X = S, Se. They all have identical crystal structure and are similar electronically. These

compounds, once available in monolayer form, will provide a chemically rich family of semiconducting atomic membranes for exploring the valley physics, as we have demonstrated here for MoS<sub>2</sub>.

## References

- [1] O. Gunawan, Y. P. Shkolnikov, K. Vakili, T. Gokmen, E. P. De Poortere, and M. Shayegan. Valley susceptibility of an interacting two-dimensional electron system. *Phys. Rev. Lett.*, 97:186404, 2006.
- [2] A. Rycerz, J. Tworzydło, and C. W. J. Beenakker. Valley filter and valley valve in graphene. *Nat. Phys.*, 3:172–175, 2007.
- [3] A. R. Akhmerov and C. W. J. Beenakker. Detection of valley polarization in graphene by a superconducting contact. *Phys. Rev. Lett.*, 98:157003, 2007.
- [4] Di Xiao, Wang Yao, and Qian Niu. Valley-contrasting physics in graphene: Magnetic moment and topological transport. *Phys. Rev. Lett.*, 99:236809, 2007.
- [5] Wang Yao, Di Xiao, and Qian Niu. Valley-dependent optoelectronics from inversion symmetry breaking. *Phys. Rev. B*, 77:235406, 2008.
- [6] K. Takashina, Y. Ono, A. Fujiwara, Y. Takahashi, and Y. Hirayama. Valley polarization in si(100) at zero magnetic field. *Phys. Rev. Lett.*, 96:236801, 2006.
- [7] N. C. Bishop, M. Padmanabhan, K. Vakili, Y. P. Shkolnikov, E. P.

- De Poortere, and M. Shayegan. Valley polarization and susceptibility of composite fermions around a filling factor  $\nu = 2/3$ . *Phys. Rev. Lett.*, 98:266404, 2007.
- [8] K. Eng, R. N. McFarland, and B. E. Kane. Integer quantum hall effect on a six-valley hydrogen-passivated silicon (111) surface. *Phys. Rev. Lett.*, 99:016801, 2007.
- [9] Zengwei Zhu, Aurelie Collaudin, Benoit Fauque, Woun Kang, and Kamran Behnia. Field-induced polarization of dirac valleys in bismuth. *Nature Phys.*, advance online publication:–, 10 2011.
- [10] Kin Fai Mak, Changgu Lee, James Hone, Jie Shan, and Tony F. Heinz. Atomically thin MoS<sub>2</sub>: A new direct-gap semiconductor. *Phys. Rev. Lett.*, 105:136805, 2010.
- [11] Andrea Splendiani, Liang Sun, Yuanbo Zhang, Tianshu Li, Jonghwan Kim, Chi-Yung Chim, Giulia Galli, and Feng Wang. Emerging photoluminescence in monolayer MoS<sub>2</sub>. *Nano Lett.*, 10:1271–1275, 2010.
- [12] Gianluca Giovannetti, Petr A. Khomyakov, Geert Brocks, Paul J. Kelly, and Jeroen van den Brink. Substrate-induced band gap in graphene on hexagonal boron nitride: *Ab initio* density functional calculations. *Phys. Rev. B*, 76:073103, 2007.
- [13] S. Y. Zhou, G. H. Gweon, A. V. Fedorov, P. N. First, W. A. de Heer, D. H. Lee, F. Guinea, A. H. Castro Neto, and A. Lanzara. Substrate-induced bandgap opening in epitaxial graphene. *Nat. Mater.*, 6:770–775, 2007.

- [14] Changgu Lee, Huguen Yan, Louis E. Brus, Tony F. Heinz, James Hone, and Sunmin Ryu. Anomalous lattice vibrations of single- and few-layer MoS<sub>2</sub>. *ACS Nano*, 4(5):2695–2700, 2010.
- [15] H. S. S. Ramakrishna Matte, A. Gomathi, Arun K. Manna, Dattatray J. Late, Ranjan Datta, Swapan K. Pati, and C. N. R. Rao. MoS<sub>2</sub> and WS<sub>2</sub> analogues of graphene. *Angew. Chem.*, 122, 2010.
- [16] B. Radisavljevic, A. Radenovic, J. Brivio, V. Giacometti, and A. Kis. Single-layer MoS<sub>2</sub> transistors. *Nat Nano*, 6:147–150, 2011.
- [17] D. M. Ceperley and B. J. Alder. Ground state of the electron gas by a stochastic method. *Phys. Rev. Lett.*, 45:566–569, 1980.
- [18] M. Gajdoš, K. Hummer, G. Kresse, J. Furthmüller, and F. Bechstedt. Linear optical properties in the projector-augmented wave methodology. *Phys. Rev. B*, 73:045112, 2006.
- [19] Robert Karplus and J. M. Luttinger. Hall effect in ferromagnetics. *Phys. Rev.*, 95:1154–1160, 1954.
- [20] Ming-Che Chang and Qian Niu. Berry phase, hyperorbits, and the hofstadter spectrum. *Phys. Rev. Lett.*, 75:1348–1351, 1995.
- [21] D. Xiao, G.-B. Liu, W. Feng, X. Xu, and W. Yao. Coupled spin and valley physics in monolayer MoS<sub>2</sub> and group-VI dichalcogenides. arXiv:1112.3144v1.